CHAPTER 2

ANALYSIS AND DESIGN OF THE QUASI-OPTICAL MODE LAUNCHERS AND RF WINDOW FOR GYROTRON

2.1. Introduction

One of the main advantages of the gyrotron oscillators is ability to operate the device in the higher order TE_{mnq} modes, thereby accruing the advantages of wide transverse dimension and generation of higher power levels at the high frequencies. However, the higher order mode interaction is not suitable due to long path transmission, plasma heating, etc. For the effective transport and controlled heating, the radiation must be converted to suitable low order waveguide modes TE_{0n}, linearly polarized HE_{11} mode, Gaussian modes in free space i.e., TEM_{00}.

Conversion of higher order modes using conventional waveguide converters is complex and lossy due to several stages of intermediated mode conversion are involved that leads longer transmission lines as well generation of the unwanted modes. In addition, these conventional mode converters are external to the device that makes the design of the collector complex; since it has to collect the spent electron beam as well as to guide the generated RF power to RF window through it. Hence, the overall efficiency of the device limited in case of high order interaction cavity modes which can be improved. This limitation causes the incorporation of axial output coupling, discussed in the Chapter 1.

In 1975, Vlasov *et al.* proposed a novel mode conversion technique that uses an internal waveguide section followed by a cut and a group of curved mirrors for the conversion of interaction mode into a small, Gaussian focused free space mode TEM_{00}. The component collectively called as quasi optical mode converter.

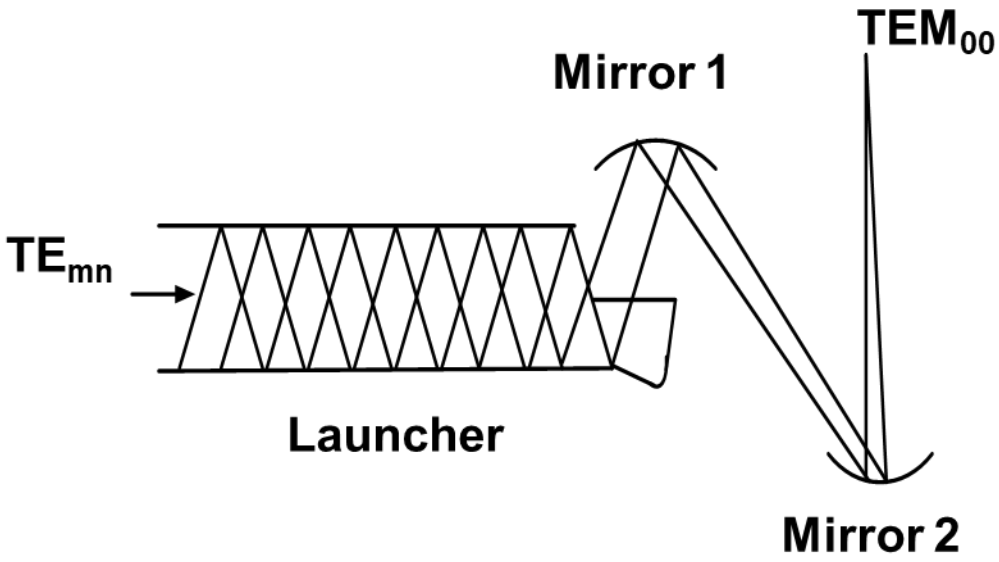

Figure 2.1: A schematic view of quasi optical mode converter system.

A Schematic view of conventional QOM Converter as shown in Figure 2.1, consists of two sections, the prime section is a Launcher, a kind of cylindrical waveguide followed by a spiral cut at its end used for launching the interaction cavity modes as a paraxial beam of radiation, and the subsequent section is mirror system used for beam focussing and shaping the launched beam into a beam of desired characteristics at the output RF window.

There are basically two types of converters which are differentiated based on the type of launcher profile, namely, Vlasov type converter, is the basic and fundamental quasi optical mode converter presented by Vlasov *et al.* and Denisov type is a modified Vlasov type converter and presented by Denisov *et al.*

Due to compactness of QOM converter over conventional mode converters, permits the incorporation of mode converter in the device and allows the separation of RF wave towards RF window and electron beam towards collector thereby

improvement of the overall efficiency of the device by depressed collector technique. An experimental investigations of the original device in which the transformation of $TE_{10,1}$ cylindrical waveguide mode to a narrow beam in free space mode was achieved with a modest power transfer efficiency of 80% using the Vlasov converter [Vlasov *et al.* (1975)].

The fundamental designs of the launcher and reflector, proposed by Vlasov *et al.* in 1975, are rooted in the geometric optics approximation. Using this theory, the propagation of the TE_{mn} mode is represented into group of rays and thereby calculation of the launcher parameters for the suitable radiation into mirrors. As well using, a rigorous vector diffraction theory was developed to calculate the radiated fields onto mirrors as well optimization of reflector/mirror surface parameters has done by the determination of Stratton Chu integrals.

Considering the conversion efficiency and the practical issues with mirror surface designs for high order TE_{mn} modes, in 1992, Denisov *et al.* proposed *a pre-bunching or pre-shaping or dimpled or rippled or Denisov converter* by modifying the launcher section of the Vlasov converters. By allowing a very small irregularities (far less than the mean radius of the launcher) on the launcher walls, the cylindrical waveguide mode coming from the cavity section is couples its power to several modes whose modes mixture gives an almost a small and Gaussian focussed beam at the launcher itself. Hence, it allows the beam shaping and focussing issues of mirrors simple and reduces the losses in the launcher section thereby more conversion efficiency.

The rippled wall waveguide is usually optimized using coupled mode theory, and the analysis used for it is described in the following sections. Various theories that

help for design, analysis of Vlasov and Denisov launchers and mirror sections are reported in the literature. AS well Launcher Optimization Tool (LOT) and SURF3D tools by J Neilson Calabazas Creek Res., Saratoga, CA, USA l [2004] are the computer codes been developed for analysis and optimization of QO launchers used in high power gyrotrons and are commercially available.

Accompanied by mode conversion, the inclusions of QOMC give numerous advantages and are follows:

I. Incorporation of depressed collector technique thereby increase in the overall efficiency of the device

II. Collection of radial output coupling, that makes collector design exclusively.

III. Reliability and protection of the device from the back propagation of RF by Vacuum RF window.

IV. Directly connect to the transmission line and reduces large dimensional transmission line system.

In the present work, with the help of the geometric optics and the coupled mode theory, the launchers used for the mode conversion of 95GHz 100kW gyrotron operating in high order $TE_{10,4}$- mode is designed and design and analysis of RF structures described in Chapter 4 of this thesis. The launchers are studied using coupled mode theory however its mirror section design is not kept within the scope of the work embodied in the present thesis. As well followed by QOMC, an RF window which is responsible for the transmission of generated power in the RF device to the transmission line is designed for the various popular window materials. Even though, the mirror is not designed here, since the design of RF window mainly dependents on the window

disc thickness and the dielectric properties of the material, using the available literature, the RF window design is attempted for a few window materials, as a tutorial exercise.

Chapter 2 is organized as follows: Starts with the importance of the quasi-optical mode converters, the analysis used for the design of Vlasov launcher is presented. Then the coupled mode theory is used for the design of the dimpled wall launcher and the theory required for the calculations of mode contents in various modes along with theory used for wall field intensities is presented briefly. Followed by the design and analysis of the Denisov launchers for $TE_{10,4}$ mode for 95GHz, 100kW is discussed. Then, the analysis and design of the RF window for the present gyrotron designs reported in the Chapters to follow are presented.

2.2. Vlasov Type Mode Launcher

For the design and analysis of quasi optical mode converters, the study of wave propagation inside an overmoded waveguide are explored by using a ray model (Fig. 2.2) that results from geometrical optics theory. We give a summary of the geometric optical parameters, a more detailed derivation can be found in [Drumm (2002), Michel (1998), and Wien 1995].

2.2.1. Geometric-optical field representation in cylindrical waveguides

We can use the scalar potential from equation to describe the wave propagation. By separating the Bessel function in into the Hankel functions of first and second kind with order *m*, we represent the standing wave in radial direction with two traveling waves.

$$J_m(x)=\frac{1}{2}\left(H_m^1(x)+H_m^2(x)\right), \tag{2.1}$$

$$\psi=\psi^{(1)}+\psi^{(2)}=\frac{1}{2}\left[H_m^{(1)}\left(k_\rho\rho\right)+H_m^{(2)}\left(k_\rho\rho\right)\right]e^{\mp jm\varphi}\,e^{\mp jk_z z}\ . \tag{2.2}$$

Furthermore, we take an adapted form of the approximation from [Morse *et al.* (1953)] for the two Hankel functions, that is valid for $x = \chi_{mn} > m$ and large arguments x and hence valid on the waveguide wall:

$$H_m^{(1),(2)}(x) \approx \sqrt{\frac{2}{\pi\sqrt{x^2-m^2}}}\, e^{\pm j\left(\sqrt{x^2-m^2}-m.\cos^{-1}\left(\frac{m}{x}\right)-\frac{\pi}{4}\right)}, \tag{2.3}$$

where the upper sign belongs to superscript (1) and the lower sign belongs to superscript (2).

By using,

$$H_m^{(1)}(x) = \left(H_m^{(2)}(x)\right)^* . \tag{2.4}$$

If we now take the gradient of the phase function of the radially outgoing wave (2) and use (2.3), we get an equation that is similar to the Eikonal equation found in [Born et al. (2009)]. This gradient vector $\vec{R}$ is perpendicular to the phase front and represents the direction of the rays. For a wave propagating in positive *z*-direction and in positive φ-direction this results in:

$$\begin{aligned}\vec{R} &= \nabla\left(\arg\left(\psi^2(R_0,\varphi,z)\right)\right) \\ &= \nabla\left(-\sqrt{(k_\rho\rho)^2-m^2}+m\cos^{-1}\left(\frac{m}{k_\rho\rho}\right)+\frac{\pi}{4}-m\varphi-k_z z\right)\Bigg|_{k_\rho\rho=\chi'_{mn}}\end{aligned} \tag{2.5}$$

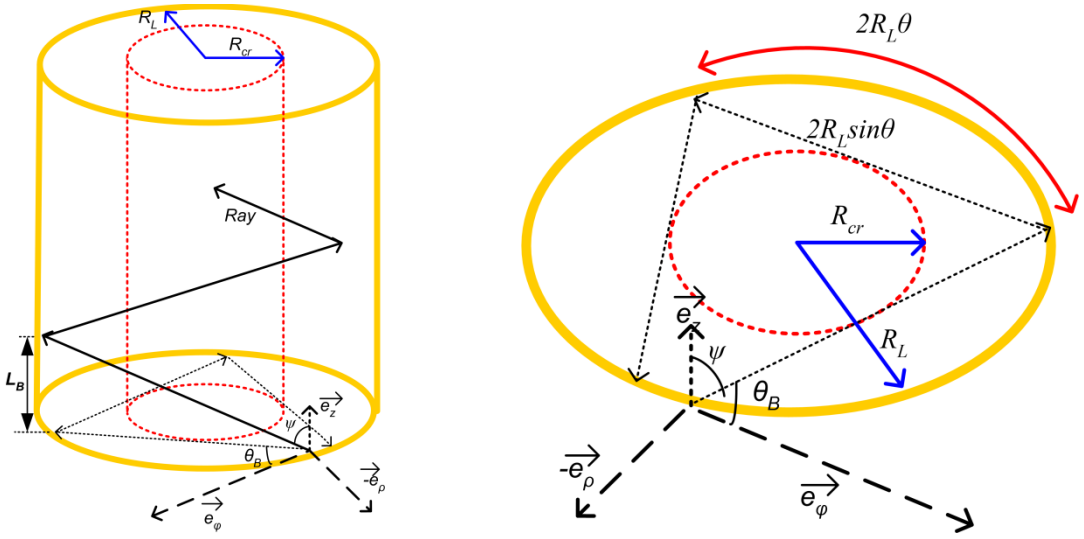

(a) (b)

Figure 2.2: Geometric optical description of a wave beam in a cylindrical waveguide (a) Side view; (b) top view.

Considering figure 2.2 and projecting this ray $\vec{R}$ onto $\vec{e}_z$, we get the so-called Brillouin angle, θ_B:

$$\cos\theta_B = \frac{k_z}{k} \quad . \tag{2.6}$$

The wave-number along the ray $\vec{R}$ is the free space wavenumber k. The distance the ray $\vec{R}$ travels in z-direction is called Brillouin length L_B shown in the left part of figure 2.2. This distance can be calculated from the TE mode's parameters as follows

$$L_B = 2R_0 \sin\alpha \cot\theta_B \quad . \tag{2.7}$$

The projection in the transverse plane onto $\vec{e}_\varphi$ yields the spread angle α as

$$\cos\alpha = \frac{m}{\chi_{mn}} = \frac{R_{cr}}{R_0} \quad , \tag{2.8}$$

where R_{cr} is the so called caustic radius [Weinstein (1969)] and the corresponding distance travelled in transverse direction, L_{trans} is defined a

$$L_{trans} = 2R_0 \sin\alpha \tag{2.9}$$

Along the circumference of the waveguide this length corresponds to:

$$L_{\varphi} = 2R_0\,\alpha \tag{2.10}$$

The wave propagation can be described as follows: An outgoing ray represented by (2) traveling towards the waveguide wall gets reflected from the metal surface and transforms into an ingoing ray represented by (1). The ingoing ray experiences a phase jump, when reaching the caustic at R_{cr}. This can be regarded as "transformation" of the ingoing ray into the outgoing ray, then the ray gets reflected again and so on. In this way the ray travels forward through the waveguide. To describe the whole field, we have to consider all rays traveling inside the waveguide.

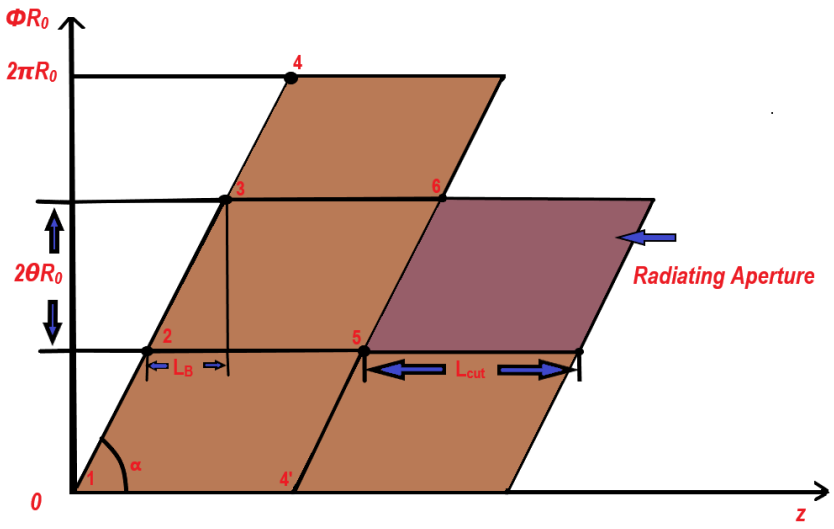

Figure 2.3: The unrolled waveguide surface at a constant radius R_0 and the Vlasov launcher cuts are highlighted.

Figure 2.3 shows the unrolled waveguide surface at a constant radius R_0. Here, we can see that all rays starting on the same helical line end on that line. So the ray

starting at point 1 travels to point 2, then to point 3, then to point $4 \equiv 4'$ and so on. It can be shown [Wien (1995)], that all rays touch the area contained within the parallelogram 2, 3, 5, 6, with size $L_{cut} \times 2\alpha R_0$ once. This area is called Brillouin zone. If we cut the waveguide open at a constant angle of ’ with length L_C, we radiate all rays as was stated before and therefore radiate all electromagnetic energy from the waveguide. As can be seen from [Wien (1995)], the cut length of a waveguide antenna in order to radiate all rays can be calculated as

$$\begin{aligned} L_{cut} &= \frac{2\pi R_0}{\tan\tau} \\ &= 2\pi R_0 \frac{\sin\alpha}{\alpha} \cot\theta_B \end{aligned} \tag{2.11}$$

with

$$\tan\tau = \frac{2R_0\,\theta_B}{L_B}\ . \tag{2.12}$$

The waveguide antenna with this type of cut achieves the separation of the electron beam from the electromagnetic wave. Thus the design of the collector of the gyrotron can be made independent of the RF output system, which is important when going to megawatt power levels.

In the geometrical optic limit, the flow of energy in a cylindrical waveguide mode can be represented by a set of rays travelling tangent to a caustic surface with an azimuthal bounce angle, α and a helical pitch angle, θ_B.

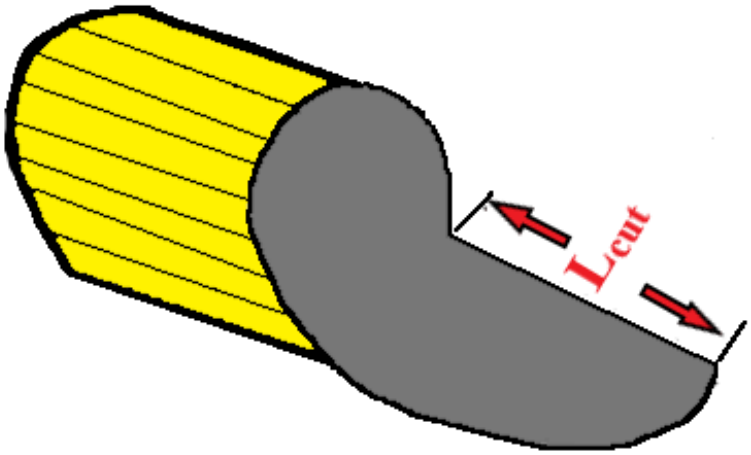

Figure 2.4: Vlasov launcher with a spiral cut of length L_{cut}.

The Stratton Chu vector diffraction theory was used to calculate the near field pattern on a plane perpendicular to the propagation direction of the launched beam. This near field pattern is determined by using the aperture fields calculated by the coupled mode theory, as the source terms in the Stratton Chu formula.

In the present Chapter, the design and analysis of converters are limited to the launcher sections only. The design and analysis of the launcher parameters for the case of single frequency gyrotron operating at 95GHz $TE_{10,4}$- mode for 100kW gyrotrons are done. In the following section, the Vlasov launcher design parameters for the current gyrotron are calculated with the help of above theories.

2.2.2. Calculations of Vlasov Launcher parameters

A Vlasov type converter is generally used for the whispering gallery interaction mode case where the radial variations of the field are upto 2. Even the role of the reflector section is very huge in this case for the beam shaping and conditioning towards the desirable beam generation. For whispering gallery modes the Vlasov type converter with a geometric optics reflector design is practical and can achieve conversion efficiencies in excess of 80%.

In the present work, the gyrotron designs are performed for TE_{62}, 95GHz, 100kW as well $TE_{10,4}$, 95GHz, 100kW which are discussed in Chapters 3 and 4, respectively. As well a low power tunable gyrotron operating in $TE_{5,3q}$ at 263 GHz presented in Chapter 6. The Vlasov launcher parameters are evaluated from the above theory and the parameters are tabulated in the Table 2.1. The dimensions of the Vlasov type launcher for the high power gyrotrons considered in the present work are tabulated in the following table.

Table 2.1: Vlasov launcher parameters

Parameter	**$TE_{6,2}$**	**$TE_{10,4}$**
Launcher radius (mm)	10	13.134
Bounce length L_B (mm)	36.1395	10.913
Bounce angle θ_B (^{o})	36.1395	65.3932
Minimum Launcher Cut length L_{cut}(mm)	71.363	30.154
Caustic radius R_{cr}(mm)	5.113	5.528
Azimuthal expansion angle 2α (^{0})	118.4955	130.2186

With the above launcher parameters the TE_{mn} mode coming from the interaction cavity is radiated as a paraxial beam on to the mirror section by providing the Vlasov cut of length L_{cut} with a azimuthal expansion angle of α. Then launched beam is guided and focussed by using the reflector section that subtend a minimum of 2α degrees, for the better conversion and focussing. In the present work, we limited our study upto launcher dimension only, not for the reflector part.

It is observed that Vlasov type converter has inherent properties that make it undesirable for converting certain classes of modes. Since the reflector must subtend a minimum of 2α degrees, the mirror for volume mode Vlasov type converters is large. Another limitation is the substantial diffraction from the Vlasov type launcher. Since,

the strong field near the cut leads larger diffraction losses and hence lowers the conversion efficiency. Even though, this smooth wall type launcher is suitable for whispering gallery mode ($m > n, n = 1, 2$), but considering the larger reflector dimensions as well lower conversion efficiency, the research has been shifted/focuses for the modified Vlasov launcher that can deliver a better conversion efficiency as well minimum diffraction losses. The modified launcher design and analysis are discussed in the following section.

2.3. Denisov Launchers

As discussed, in the Vlasov type converter, the fields are needed to radiate from the cut for the beam shaping and propagation towards reflector surfaces. But the strong fields near the cut leads severe diffraction losses and results a limited mode conversion thereby degradation of the efficiency and so not suitable for higher power sources where the efficiency matters. In addition, the requirement of the reflector surface increased as the bounce angle of the beam increases that leads the complexity and large dimensional surfaces that makes the realisation impractical. Thus, Vlasov launchers find limited use as well not potential for the conversion of high order volumetric modes. The fields along the helical cut and straight edges are very strong in Vlasov converter and that leads to strong diffraction losses there by reduction in the overall efficiency. One key idea to increase the conversion efficiency as well some decrement in the reflector dimensions is by modifying or reshaping the mode into desired mode before radiating from the cute that has very low field nearby cut in the launcher itself. Later on, by using reflector section, the radiated beam is shaped into desired form. In 1992, Denisov have proposed a technique to reduce the fields along the helical and straight cut edges by deforming the waveguide walls. The deformations of the waveguide walls allow the

coupling of the main mode energy into several modes and the interference of these modes on the launcher walls allows Gaussian bundles mixture formation since the Gaussian bundles have less or almost no fields at the edges of Brillouin regions and causes less or no diffraction achieves maximum conversion efficiency.

An ideal TE_{mn} mode converted into a perfect Gaussian beam mode through a profiled launcher by allowing the mixture of several modes in desired proportions of power as tabulated in the Table 2.2 at the launcher end.

Table 2.2: Ideal proportions of satellite mode mixture of a dimpled launcher

$TE_{m+2,n-1}$ (3%)	$TE_{m+3,n-1}$ (11%)	$TE_{m+4,n-1}$ (3%)
$TE_{m-1,n}$ (11%)	**$TE_{m,n}$ (44%)**	$TE_{m+1,n}$ (11%)
$TE_{m-4,n+1}$ (3%)	$TE_{m-3,n+1}$ (11%)	$TE_{m-2,n+1}$ (3%)

The interference of the nine wave guide modes creates an RF field bunching in the longitudinal and azimuthal directions. Selection of these modes are depends on the caustic radii, interference length of modes close to the cut length L_{cut} and similar Bessel zeros close to the interaction cavity mode $TE_{m,n}$.

Followings are the most common used Denisov launcher profiles for the reshaping of the cavity mode into Gaussian beam mode in the launcher itself.

$$R(\phi, z) = R_0 + \alpha_L z + \delta_1(z)\cos(\Delta\beta_1 z - L_1\phi) + \delta_2(z)\cos(\Delta\beta_2 z - L_2\phi) \tag{2.13}$$

$$R(\phi, z) = R_0 + \alpha_L z + \delta_1(z)\cos(\Delta\beta_1 z + L_1\phi) + \delta_2(z)\cos(\Delta\beta_2 z + L_2\phi) \tag{2.14}$$

$$R(\phi, z) = R_0 + \alpha_L z + \delta_1(z)\sin(\Delta\beta_1 z - L_1\phi) + \delta_2(z)\sin(\Delta\beta_2 z - L_2\phi)\,. \tag{2.15}$$

Here the parameters $\Delta\beta_{1,2}$ and $L_{1,2}$ are dependents on the selection satellite modes that are responsible for the Gaussian mode formation by azimuthal and radial bunching of the modes [Kartikeyan *et al.* (2004)]. Values of $\alpha, \delta_1(z), \delta_2(z)$ are chosen such that the desired proportions of couplings between the modes are achieved with minimum lengths and α_L is the small taper angle added to the radius of the launcher profile to avoid counterfeit oscillations in the launcher.

The overall bunching of Gaussian beam formed by superposition of azimuthal bunching , caused by the satellite modes that have equal caustic radii (R_{cr}) and similar Bessel zeros (χ_{mn}) and longitudinal bunching by the satellite modes that have equal caustic radii (R_{cr}) and an interference length close to the Launcher cut length L_{cut}, along the launcher section. L_1 and L_2 are the differences in the azimuthal indices of the main and satellite modes [Blank (1994)].

Practically, it is difficult to achieve the above said mode mixture with accuracy, but keeping it as our target, the profile has been optimized such that it results a Gaussian content at the cut of more than 99%. The theory required for mode variations and calculations of Gaussian content factor due to a dimpled mode waveguide sections are discussed below.

The parameters of several Denisov launcher profiles used and implemented in the literature are mentioned in Table 2.3 [Flamm (2012)].

Table 2.3: Various dimpled profiles [Flamm (2012), Blank (1994)]

f (GHz), mode	R_0/L (mm)	α_L	Type	L_1/L_2	$\delta_1(z)$,mm	$\delta_2(z)$,mm
118, $TE_{22,6}$	20/200	2e-3	2.13	1/3	$\begin{cases} 0\,to\,0.05, & 0<z<10 \\ 0.05, & 10<z<80 \\ 0.05\,to\,0, & 80<z<90 \\ 0, & else \end{cases}$	$\begin{cases} 0\,to\,0.05, & 10<z<20 \\ 0.05, & 20<z<90 \\ 0.05\ to\,0, & 90<z<100 \\ 0, & else \end{cases}$
110, $TE_{22,6}$	20/152	0	2.14	1/3	0.0399	0.0399
140, $TE_{28,8}$	21.9/250	4e-3	2.13	1/3	$\begin{cases} 0\,to\,0.041, & 0<z<10 \\ 0.041, & 10<z<60 \\ 0.05\,to\,0, & 60<z<70 \\ 0, & else \end{cases}$	$\begin{cases} 0\,to\,0.041, & 17<z<27 \\ 0.041, & 27<z<77 \\ 0.041\,to\ 0, & 77<z<87 \\ 0, & else \end{cases}$

2.3.1. Analysis of the dimpled launcher

Since the launcher waveguide walls have deformations that allow the coupling between modes, so cannot represent the energy through one normal mode. The study of coupling of energy between modes in these waveguides can be handled well with the help of coupled mode theory which gives the variations of the modes along the direction of the propagation. It is the goal of the pre bunching waveguide section to improve the radiation characteristics of the launched beam by illuminating the launching region (B') with a Gaussian ray distribution rather than a uniform distribution. The fields radiated into free space are coming from the Brillouin region just before the Brillouin region removed for launching the beam. Radiating aperture is the portion of the waveguide that is responsible for launching the beam. Hence, with the help of fields on the

Brillouin region just before the cut, the radiated fields at an observation point can be studied. Hence, in the study of the launchers, need to achieve good Gaussian content factors at two successive Brillouin regions for efficient conversion.

Hence, now days almost all the gyrotron device incorporate Denisov type converter as an internal part considering high order operating mods as well requirement of no power loss in the mode conversion.

Generally, the profile of Denisov launcher is a deformed one. Since the wall shapes are changing continuously, the fields in the waveguide cannot be represented through one normal mode and the deformations allows coupling of energy between different normal modes of the waveguide. This peculiar situation can be handled with the help of coupled mode theory which calculates the coupling coefficients of mode due to deformations in the structure. Coupled mode theory tells the coupling among the modes due to variations in the structure. If the amount of perturbation is very small compared to the mean radius of the waveguide, then can neglect the backward wave propagation.

In general, the coupling between forward travelling modes are given by the following expressions:

$$\frac{dA_i^+}{dz} = -ik_{zi}A_i^+ + \sum_u c_{iu}A_u^+ + \sum_v c_{iv}A_v^+, \tag{2.16}$$

$$\frac{dA_j^+}{dz} = -ik_{zj}A_j^+ + \sum_u c_{ju}A_u^+ + \sum_v c_{jv}A_v^+, \tag{2.17}$$

where the subscripts i and u deals for TE modes and the subscripts j and v for TM modes. A is the complex amplitude of the mode. For weak waveguide deformations of

the form $R(\phi, z) = R_0 + \delta(\phi, z)$ previously reported methods [Blank *et al.* (1994)] can be used determine the coupling coefficients for mild perturbations. The coupling coefficients, c_{iu}, c_{iv}, c_{ju}, and c_{jv} can be represented as follows:

$$c_{iu} = \frac{1}{2}\left[Q_{iu} \frac{\omega\mu}{\sqrt{k_{zi} k_{zu}}} + R_{iu} \sqrt{\frac{k_{zu}}{k_{zi}}} \right], \tag{2.18}$$

$$c_{iv} = \frac{1}{2} S_{iv} \frac{\omega}{c\sqrt{k_{zi} k_{zv}}} , \tag{2.19}$$

$$c_{ju} = \frac{1}{2}\left[T_{ju} c \sqrt{\frac{k_{zj}}{k_{zu}}} + U_{ju} \frac{1}{c} \sqrt{\frac{k_{zu}}{k_{zj}}} + V_{ju} \frac{c}{\omega} \sqrt{k_{zj} k_{zu}} \right] , \tag{2.20}$$

and

$$c_{jv} = \frac{1}{2}\left[W_{jv} \sqrt{\frac{k_{zj}}{k_{zv}}} + X_{jv} \frac{\omega\varepsilon}{\sqrt{k_{zj} k_{zv}}} \right] . \tag{2.21}$$

The term c_{mn} gives the coupling coefficient from the n^{th} mode of, TE or TM type to m^{th} mode of TE or TM type.

For a small amplitude perturbation of first order, $\delta(\phi, z)$, the eight unknowns in coupling coefficient expressions, (2.18) to (2.21) can studied with the help of [Doane (1985), Doane (1986) and Garin *et al.* (1987)]. Here, considering , the subscripts *i, u, j*, and *v*, refer to mode *i, u, j,* and *v*, where mode *i* is the $TE_{m_1 n_1}$, mode *u* is the $TE_{m_2 p_2}$, mode *i* is the $TM_{m_1' p_1'}$ and mode *v* is the $TM_{m_2' n_2'}$. The unknowns in equations. (2.18) to (2.21) are determined from the following expressions:

$$Q_{iu} = \frac{i\left(\frac{\nu_{m_2 p_2}}{R_0}\right)^2}{R_0 \pi \omega \mu \sqrt{\nu_{m_2 p_2}^2 - m_2^2}} \int_0^{2\pi} \left[\frac{i m_1 e^{i m_1 \phi}}{\sqrt{\nu_{m_1 p_1}^2 - m_1^2}} \frac{\partial \delta(\phi, z)}{\partial \phi} + \delta(\phi, z) e^{i m_1 \phi} \sqrt{\nu_{m_1 p_1}^2 - m_1^2} \right] e^{-i m_2 \phi} d\phi \tag{2.22}$$

$$R_{iu} = \frac{m_1 m_2}{R_0 \pi \sqrt{\nu_{m_1 p_1}^2 - m_1^2} \sqrt{\nu_{m_2 p_2}^2 - m_2^2}} \int_0^{2\pi} e^{i m_1 \phi} e^{-i m_2 \phi} \frac{\partial \delta(\phi, z)}{\partial z} d\phi \tag{2.23}$$

$$S_{iv} = \frac{i m_1}{R_0 \pi \sqrt{\nu_{m_1 p_1}^2 - m_1^2}} \int_0^{2\pi} e^{i m_1 \phi} e^{-i m_2^l \phi} \frac{\partial \delta(\phi, z)}{\partial z} d\phi \tag{2.24}$$

$$T_{ju} = \frac{i\left(\frac{\nu_{m_2 p_2}}{R_0}\right)^2}{R_0 \pi \omega \mu \sqrt{\nu_{m_2 p_2}^2 - m_2^2}} \int_0^{2\pi} \left[e^{i m_1^l \phi} \frac{\partial \delta(\phi, z)}{\partial \phi} + i m_1^1 e^{i m_1 \phi} \delta(\phi, z) \right] e^{-i m_2 \phi} d\phi \tag{2.25}$$

$$U_{ju} = \frac{m_2}{R_0 \pi \omega \varepsilon \sqrt{\nu_{m_2 p_2}^2 - m_2^2}} \left(\frac{\mu_{m_1^1 p_1^1}}{R_0} \right) \int_0^{2\pi} e^{i m_1^l \phi} e^{-i m_2 \phi} \delta(\phi, z) d\phi \tag{2.26}$$

$$V_{ju} = \frac{-i m_2}{R_0 \pi \sqrt{\nu_{m_2 p_2}^2 - m_2^2}} \int_0^{2\pi} e^{i m_1^l \phi} e^{-i m_2 \phi} \frac{\partial \delta(\phi, z)}{\partial z} d\phi \tag{2.27}$$

$$W_{jv} = \frac{1}{R_0 \pi} \int_0^{2\pi} e^{i m_1^l \phi} e^{-i m_2^1 \phi} \frac{\partial \delta(\phi, z)}{\partial z} d\phi \tag{2.28}$$

$$X_{jv} = \frac{i}{R_0 \pi \omega \varepsilon} \left(\frac{\mu_{m_1^1 p_1^1}}{R_0} \right) \int_0^{2\pi} e^{i m_1^l \phi} e^{-i m_2^l \phi} \delta(\phi, z) d\phi \tag{2.29}$$

Here R_0 is the mean radius of the waveguide, μ_{mp} and ν_{mp} are the p^{th} zero of $J_m(x)$ and $J_m^1(x)$, respectively.

The set of equations from 2.16 -2.29, gives the complete study of mode coupling caused by the irregularities whose amplitudes are of the order $\delta << R_0$ successfully. Though, in the gyrotrons the oscillation of TM_{mn} modes are not feasible in the interaction as well considering the amount of dimples, only coupling between TEmn are happens. Hence, using equation 2.16, 2.18, 2.22, and 2.23 together, the mode variations along the dimpled launcher can be determined successfully.

Observing the mode variation profiles the probable set of dimple launcher can be selected and will be confirmed by calculating the correlation coefficient of the Gaussian content of the wall field intensity near cut. The necessary theories are presented below.

2.3.2. Calculation of waveguide field components

The energy in the waveguide cannot sufficiently represent by single normal mode field components if the waveguide walls are changing continuously, i. e., nonuniform waveguide. Because of non-uniformity, there is always coupling of energy among several modes. If the amount of perturbations are mild, i. e., very small compared to mean radius of the waveguide, then the coupling between different kind of modes can be neglected, i. e., between TE and TM modes. Since, our Denisov type converter is used as an internal component of the gyrotrons which generates power in the TE_{mp} cavity modes. Hence, the calculation of TM mode effects is irrelevant here. Because of small non-uniformities, the overall field components can be calculated as a superposition of the forward travelling modes which assume propagate in the waveguide. The overall *E* and *H* fields in deformed waveguide walls are calculated with the following expression [Zhang *et al.* (2015)]:

$$H = \sum_i A_i^+(z)\, h_i\, e^{-j\int_0^z \beta_i z^1 dz}, \qquad (2.30)$$

$$E = \sum_i A_i^+(z)\, e_i\, e^{-j\int_0^z \beta_i z^1 dz}, \tag{2.31}$$

and,
$$\iint_s e_i \times h_j \, ds = \pm\delta_{ij}, \tag{2.32}$$

where A_i^+ amplitude of the TE_{mp}, and it carries attenuation term with it but does not have the oscillation term. e_i and h_j are the orthogonal fields in the circle waveguide, s is the cross section and δ_{ij} is Dirac's delta function. And the term $e^{-j\int_0^z \beta_i z^1 dz}$ is the oscillation term and it is z dependent because the waveguide radius under consideration is varying with the z.

When the amplitude of the deformation is very smaller compared to mean radius of the waveguide, the TE_{mn} components in the circular waveguide for right hand rotating wave can be written as:

$$T_i = \frac{k}{\sqrt{\pi\beta_m}\sqrt{\chi_{mp}^2 - m^2 J_m(\chi_{mp})}} J_m\left(\frac{\chi_{mp} r}{R_0}\right) e^{-im\phi}. \tag{2.33}$$

Here k is free space wavenumber, r and φ are the radial and azimuthal coordinates, R_0 is the mean waveguide radius, β_m is the transverse wavenumber, χ_{mp} is the n^{th} root of the Bessel function, $J_m^l(\chi_{mp}) = 0$. With the help of T_i, the orthogonal fields can be expressed as follows:

$$e_i = \sqrt{\frac{\mu\omega}{\beta}}\left(\frac{1}{r}\frac{\partial T}{\partial \phi}\, a_r + \frac{\partial T}{\partial r} a_\phi\right), \tag{2.34}$$

$$h_i = \sqrt{\frac{\beta_m}{\mu\omega}}\left(\frac{\partial T_i}{\partial r} a_r + \frac{1}{r}\frac{\partial T_i}{\partial \phi} a_\phi + j\frac{\chi_{mp} m^2 T_i}{k^2 R_0^2} a_z\right). \tag{2.35}$$

Here a_r, a_φ, and a_z are the orthogonal unit vectors in radial, azimuthal and axial directions. With the help of equations (2.30) to (2.35), the fields on the deformed waveguide walls can be determined if the amplitudes of the modes are known. Hence, by the combination of coupled mode theory and super position concepts, the mode variation profiles along the axial direction as well as the field components of the deformed waveguide walls can be studied.

The following section is dedicated to the derivation of the required theory, necessary to describe the wave propagation in launchers.

Since the goal is to radiate the electromagnetic wave from the waveguide cut in the form of a Gaussian beam (Section 2.2), we need to obtain a mixture of different modes to form the Gaussian field profile. Consequently the electromagnetic wave will not consist of one single electromagnetic mode, but a linear combination of different modes. This can be achieved by summing over the azimuthal indices m and integrating over the longitudinal wave numbers k_z, see [Harrington (1961)]:

$$\psi(\rho,\varphi,z)=\sum_m \int_{k_z} A_{mn}(k_z)\, J_m\left(\sqrt{k^2-k_z^2}\,\rho\right) e^{-jm\varphi}\, e^{-jk_z z}\, dk_z . \qquad (2.36)$$

The previous derivations were made for TE as well as TM modes. However in the following only TE modes will be considered. The only source for TM modes is mode conversion, which will be neglected due to the smooth change in the waveguide surface.

The quality of launcher performance is analyzed by calculating the Gaussian beam content at the launcher cut. The generated Gaussian beam is compared with an ideal Gaussian beam and the content factor is measured and is given by

$$\eta_{scalar} = \frac{\left(\iint_S |u_1|.|u_2| \, dS \right)^2}{\iint_S |u_1|^2 dS . \iint_S |u_2|^2 dS}, \tag{2.37}$$

$$\eta_{vector} = \frac{\left| \iint_S u_1^* . u_2 \, dS \right|^2}{\iint_S |u_1|^2 dS . \iint_S |u_2|^2 dS} \tag{2.38}$$

where S is the aperture surface that contains the radiated Gaussian beam. Equation 2.36 compares the amplitudes of two field components u_1 and u_2 with respect to power, whereas equation 2.37 includes the phase of the field component in the comparison.

With the sufficient knowledge of the coupled mode theory and the concepts required for the calculation of the wall field intensities, the analysis and design of the dimpled mode launchers for the proposed gyrotron $TE_{10,4}$- 95 GHz and 100kW designs are carried out by developing a numerical code in the Matlab domain.

2.4. Field Computations, Results and Discussion of Denisov launchers

As per the coupled mode theory presented above, we developed a numerical code for calculation of the mode variation profiles as well wall field intensities on the launcher walls.

2.4.1. Validation of Dimpled Launcher design for $TE_{22,6}$ mode at 110GHz

In the present work, starts with the reported values given by Blank (1994), for a Denisov launcher at 110 GHz $TE_{22,6}$ mode, the mode variation profiles and the corresponding wall field intensities are determined. It was reported that, the author has shown the mode variation calculation by considering a 4 satellite modes for the launcher

profile calculation and left the consideration second category satellite modes ($TE_{m-4,n+1}$, $TE_{m-4,n-1}$, $TE_{m-4,n+1}$, and $TE_{m-2,n+1}$) though these modes generates in the launcher section and participates in the mode coupling. As well it is advised to consider more number of modes for better accuracy and optimized design.

The profile details are taken from Blank (1994) are also tabulated in Table 2.3, the mode variation profile for 4 satellite modes are done initially. Due to the irregularities in the launcher also allows coupling with the second order satellite modes, mode coupling in the structure is determined by considering more satellite modes.

As mentioned in the several occasions that LOT and SURF3D tools are used for the design and optimization of converters which are commercially available and financially expensive. In the present work, using the above mentioned theories, i.e., coupled mode theories and fied calculations in the waveguide launchers, we developed a numerical code using Matlab tool, that calculates the mode couplings across the dimpled launchers for various deformed profiles and using this mode coupling coefficients, the wall field intestines are calculated. Followed by calculation of the Gaussian content available at the launcher cut has been done for the optimization of the launcher profile. The decision on the optimization deformed surface has been taken by observing the amount of mode couplings at the end of the structure as well the Gaussian content factor at the launcher cut. All the analysis has been done by a self-numerical code in the Matlab environment.

After a successful understanding of the theories and by developing numerical code, a reported dimpled launcher profile for $TE_{22,6}$ 110GHz given by Blank (1994) has been validated.

2.4.1a. With four satellite modes

It has been observed that the mode variation profiles and the wall field intensities calculations along the launcher wall had been shown for the four primary satellite modes i.e., $TE_{19,7}$, $TE_{25,5}$, $TE_{21,6}$,and $TE_{23,6}$. At first, using self-developed code, the calculated results are plotted in Figure 2.5 and 2.6 and the results are found in good agreement with almost 100% match with the reported results.

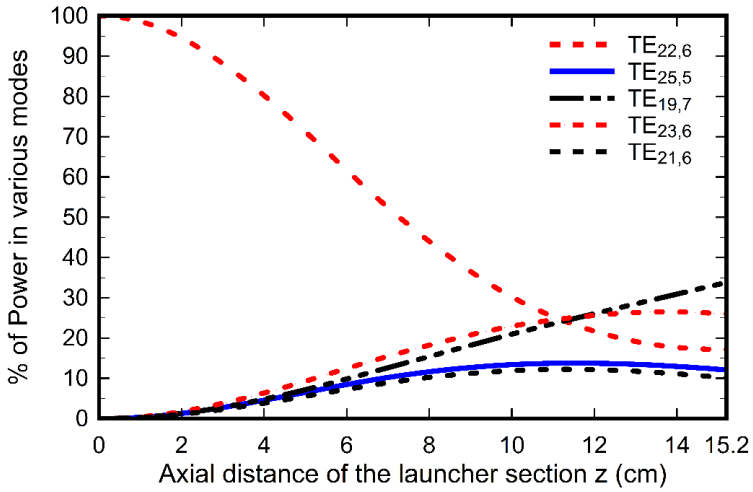

Figure 2.5: Mode variations profile along the length of the $TE_{22,6}$ mode at 110GHz launcher for eight satellite modes.

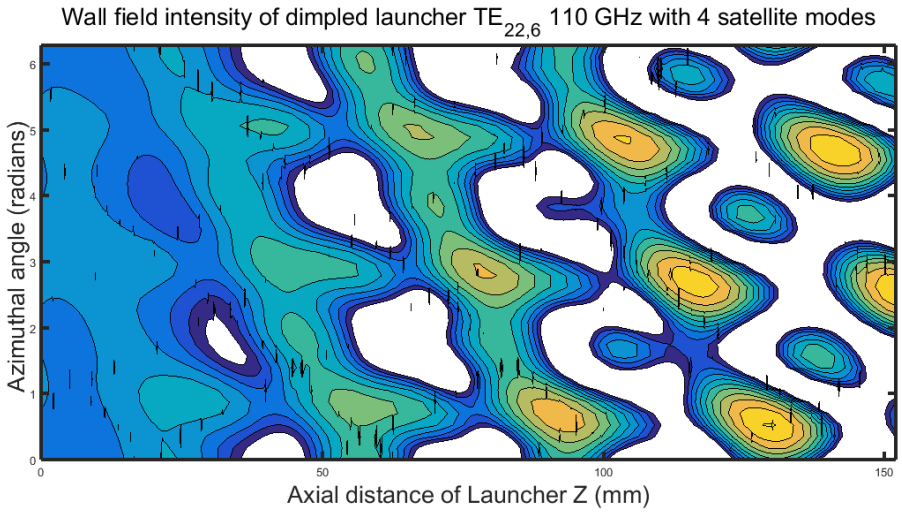

Figure 2.6: Wall field intensities on the dimple launcher of $TE_{22,6}$ mode at 110GHz for four satellite modes.

2.4.1b. With Eight satellite modes

Since, the amplitude of the deformation profiles are based on the primary satellite modes and the chosen 4 satellite modes certainly helps the growth of several modes and specially other four satellite modes ($TE_{26,5}$, $TE_{24,5}$, $TE_{23,7}$,and $TE_{18,7}$) as mentioned in Table 2.2.

We have re-calculated the mode variation profiles and the wall field intensities allowing other 4 satellite modes for more accurate study and are plotted in figures 2.7 and 2.8.

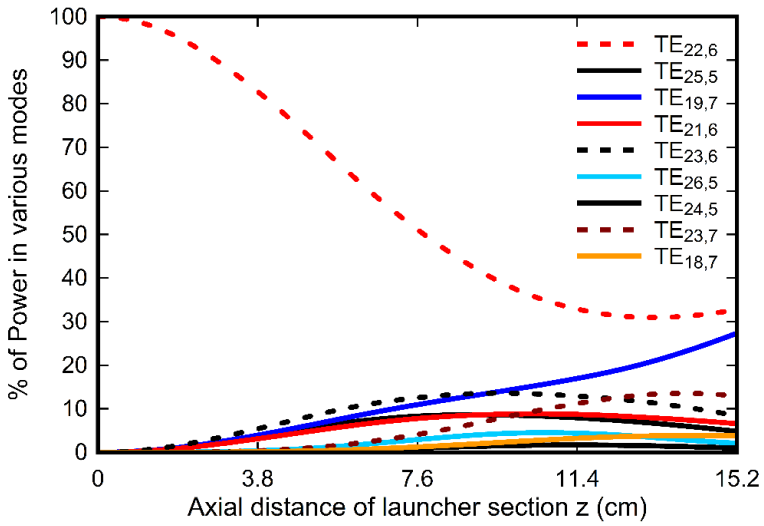

Figure 2.7: Mode variations profile along the length of the TE22,6 mode at 110GHz launcher for eight satellite modes.

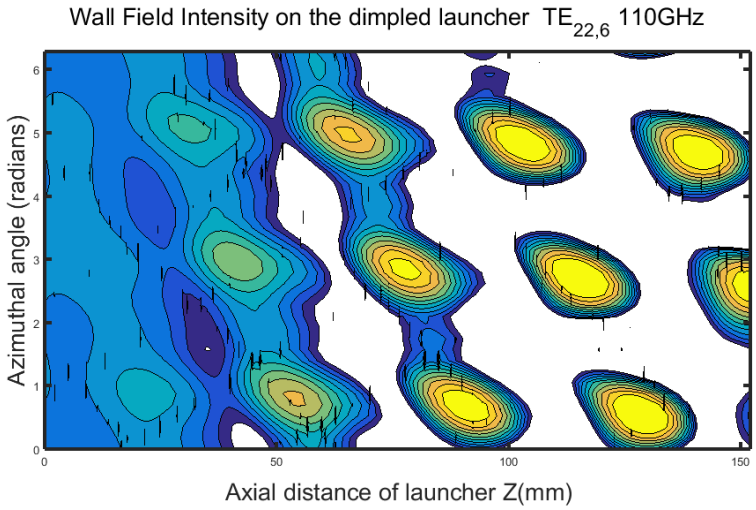

Figure 2.8: Wall field intensities on the dimple launcher of $TE_{22,6}$ mode at 110GHz for eight satellite modes.

It is observed that allowing more satellite modes in the calculations gives a different variation profile than earlier one but both cases leads to a good Gaussian beam formation at the launcher cut (on Brillouin regions). All the variations have been show pictorially.

It is perceived from figures 2.5 - 2.8 that due to second order satellite modes consideration, the amount of power in the various modes are differed significantly specially, main mode has a mode content of ~31% over 18% in the initial calculations. As well, a clear Gaussian beam can be observed in the latter case. Though, the design was the optimized and most suitable, but consideration of more satellite modes in the optimization of launcher profiles improves more accuracy and visualization of mode coupling that results a good Gaussian beam.

Further from figures 2.5 and 2.7, that even though ideal mode mixture content do not results but the optimized profiles gives a good Gaussian content near the cut. Though, it was reported that the author has allowed more satellite mods while optimizing surface but mode variations has been shown for 4 satellite modes case.

Though ideal combination of mode mixture is not realizable all the time but close to it for the optimized performance is sufficient.

2.4.2. Dimpled Launcher design for $TE_{10,4}$ mode at 95GHz

For our present design, a Denisov mode launcher design for the 95GHz, $TE_{10,4}$ mode is performed manually changing the launcher profile and confirming by observing the mode variation profile and Gaussian content at the launcher cut, since we do not have access to LOT code. Instead applying the constant dimples throughout launcher, an individual deformation profiles that results azimuthal and longitudinal bunching along with a small taper angle α_L is also, thereby Gaussian beam like mode at the launcher surface are considered for the present design. As well, the profiles are optimized by observing the mode coupling contents at the end of the launcher followed by wall field intensities. The optimized deformation profiles are plotted in figure 2.9.

The optimized dimpled profile is of nature represented by 2.13, with α_L =0.0015 and the deformed surfaces are shown in figure 2.9.

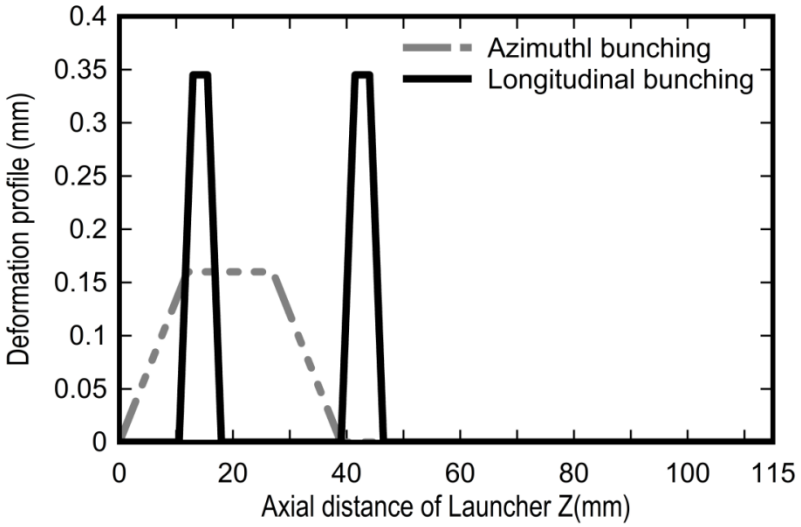

Figure 2.9: Wall Deformation profiles for the $TE_{10,4}$ mode at 95GHz launcher.

The mode variation profiles as well wall field intensities for the optimized launcher are plotted in figure 2.10-2.11.

Table 2.4: Dimpled Launcher parameters for 95GHz, $TE_{10,4}$

Parameter	**Value**
Operating mode	$TE_{10,4}$
Frequency	95GHz
Launcher Radius R_0	13.134 mm
Taper angle α_L	0.0015
Axial length of launcher	115.2 mm

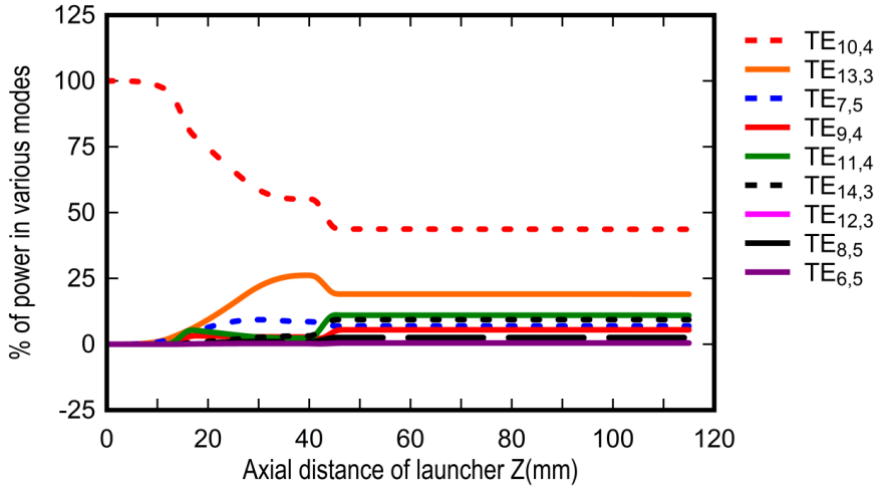

Figure 2.10: Mode variations profile along the length of the $TE_{10,4}$ mode at 95GHz launcher.

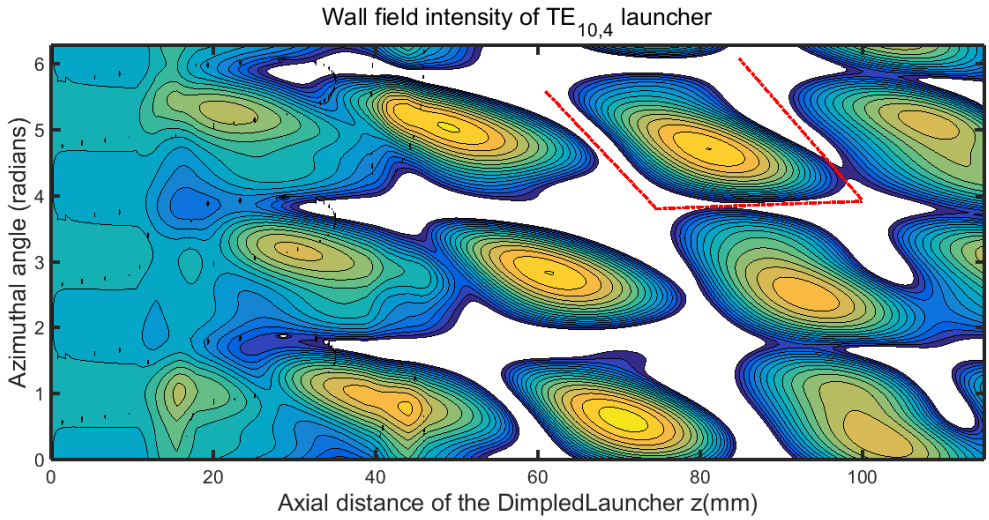

Figure 2.11: Wall field intensities on the dimple launcher of $TE_{10,4}$ mode at 95GHz.

The optimized launcher results a scalar Gaussian of more than 99% and with launcher cut has been highlighted in the figure 2.11.

2.5. Analysis and Design of Output RF Window

The RF window is an essential component of the output system of the gyrotrons and serves as a barrier between the vacuum side of the device and the external transmission line system. The desired features of an RF window are high power handling capability, high thermal conductivity and good mechanical strengths, as well large bandwidth, low reflection loss, etc.

Therefore, a proper window material with suitable geometrical and material properties is crucial for a gyrotron oscillators operating at high power and high frequencies. Usually, a low loss tangent (tan δ), high thermal conductivity, moderate mechanical strength are preferred.

In the high power Gyrotrons, materials, such as, Sapphire, Chemical vapor deposited (CVD) diamond, Silicon nitride composite, BeO, Au-doped silicon etc., are commonly used for window applications. The CVD diamond is the foremost choice for the MW power levels due to its excellent dielectric and mechanical properties. Coming

to the types of RF windows based on the construction, Disc type and Diamond windows for single and step tunable frequencies whereas Brewster windows for broadband frequencies.

In the present work, taking several materials individually, the RF window parameters are determined for the TEM_{00} mode, which is coming from the Denisov launcher that converts the $TE_{10,4}$ mode at 95GHz for 100kW power levels. The basic analytical concept used for the optimization of RF window for fixed frequency based on scattering matrix for disc type windows id briefly described here followed by the numerical calculations of the reflection and transmission characteristics for window discs of many thicknesses [Nickel *et al.* (1995)]. These results are discussed in the results and discussion section at the end of this current section.

2.5.1. Disc Type Windows

An RF window of disc type is usually characterized by disc thickness, loss tangent, disc diameter, and spacing between disc for multi disc type windows. For the disk type window, the thickness d_w is obtained by $d_w = n\lambda / 2(\varepsilon_r)^{1/2}$.

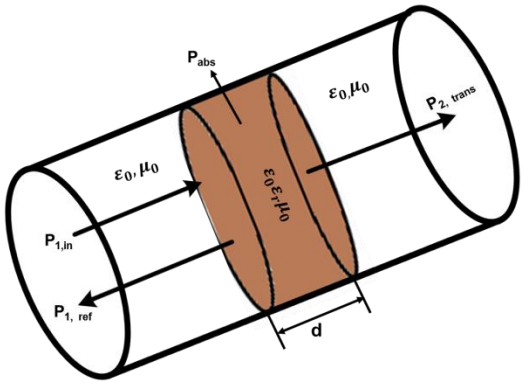

Figure 2.12: Schematic diagram of single disc type window of thickness d_w.

Figure 2.12 shows a homogeneous waveguide of arbitrary cross section with ideal conductive walls of section of the plane-parallel window of thickness *d*. The window surfaces are transverse to the waveguide axis and the disk edge is flush with the

waveguide wall. The disc is considered as it consists of one lossy homogeneous and isotropic dielectric material with the complex relative permittivity $\varepsilon_r = \varepsilon_r^{'} - j\varepsilon_r^{''} = \varepsilon_r^{'}(1 - j\tan\delta)$ and complex relative permeability $\mu_r = 1$. Nowadays, multi disc type windows where the dielectric materials are separated by a space s_d are used for the broadband applications.

Analysis of the disc type waveguide windows for gyrotrons is developed on the scattering matrix formulation and described in terms of the incident, reflected and transmitted waves. The basic formalism for disc type windows explained as follows:

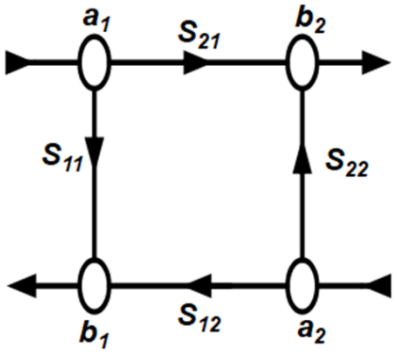

Figure 2.13: Equivalent Two port scattering matrix network.

Figure 2.13 shows an single disc waveguide window with its equivalent two-port scattering matrix network representation illustrating the incident and reflected waves a_k and b_k (k = 1, 2), respectively. The incident and reflected waves at the window plane are represented by a set of equations in matrix form as

$$[S] \equiv \begin{bmatrix} S_{11} & S_{12} \\ S_{21} & S_{22} \end{bmatrix} \equiv \begin{bmatrix} \left.\frac{b_1}{a_1}\right|_{a_2=0} & \left.\frac{b_1}{a_2}\right|_{a_1=0} \\ \left.\frac{b_2}{a_1}\right|_{a_2=0} & \left.\frac{b_2}{a_2}\right|_{a_1=0} \end{bmatrix} \tag{2.39}$$

$$\begin{aligned} b_1 &= S_{11}a_1 + S_{12}a_2 \\ b_2 &= S_{21}a_1 + S_{22}a_2 \end{aligned} . \tag{2.40}$$

The reflection, transmission and absorption coefficients in terms of the S-parameters of the network are related as:

$$R = |S_{11}|^2 = \frac{|b_1|^2}{|a_1|^2}\Big|_{a_2=0} = \frac{P_{1,refl}}{P_{1,in}}\Big|_{P_{2,in}=0} \tag{2.41}$$

$$T = |S_{21}|^2 = \frac{|b_2|^2}{|a_1|^2}\Big|_{a_2=0} = \frac{P_{2,trans}}{P_{1,in}}\Big|_{P_{2,in}=0} \tag{2.42}$$

$$A = 1 - |S_{11}|^2 - |S_{21}|^2 = \frac{P_{1,in} - P_{1,refl} - P_{2,trans}}{P_{1,in}}\Big|_{P_{2,in}=0} = \frac{P_{abs}}{P_{1,in}}\Big|_{P_{2,in}=0}. \tag{2.43}$$

The scattering matrix [S] of a dielectric region filled by material of length d_w and permittivity $\mathcal{E}$ is given by:

$$[S] = \frac{1}{1-\rho_v^2 e^{-2\gamma_{\varepsilon v} d_w}} \begin{bmatrix} \rho_v(1-e^{-2\gamma_{\varepsilon v} d_w}) & (1-\rho_v^2)e^{-\gamma_{\varepsilon v} d_w} \\ (1-\rho_v^2)e^{-\gamma_{\varepsilon v} d_w} & \rho_v(1-e^{-2\gamma_{\varepsilon v} d_w}) \end{bmatrix}, \tag{2.44}$$

where, the propagation constant $\gamma_{\varepsilon v} = \alpha_{\varepsilon v} + j\beta_{\varepsilon v} = \sqrt{k_{cv}^2 - \varepsilon_r k_0^2}$, the complex permittivity is given by $\varepsilon_r = \varepsilon_r' - j\varepsilon_r'' = \varepsilon_r'(1 - j\tan\delta)$.

$$\beta_{\varepsilon v} = \sqrt{k_0^2 \varepsilon_r' - k_{cv}^2} \cdot \sqrt{\frac{1}{2} + \frac{1}{2}\sqrt{\left(\frac{\varepsilon_r' \tan\delta}{\varepsilon_r' - (k_{cv}/k_0)^2}\right)^2 + 1}} \overset{\tan\delta << 1}{\approx} \sqrt{k_0^2 \varepsilon_r' - k_{cv}^2} \tag{2.45}$$

$$\alpha_{\varepsilon v} = \frac{k_0^2 \varepsilon_r' \tan\delta}{2\beta_{\varepsilon v}} \overset{\tan\delta << 1}{\approx} \frac{k_0 \varepsilon_r' \tan\delta}{2\sqrt{\varepsilon_r' - (k_{cv}^2/k_0)^2}} \quad . \tag{2.46}$$

The complex reflection coefficient due to the wave impedance discontinuity at the single dielectric transition plane for TE_{mn}, TM_{mn} and TEM_{00} modes are given by

$$\rho_v = \frac{\sqrt{1-(k_{cv}/k_0)^2} - \sqrt{\varepsilon_r - (k_{cv}/k_0)^2}}{\sqrt{1-(k_{cv}/k_0)^2} + \sqrt{\varepsilon_r - (k_{cv}/k_0)^2}}, \tag{2.47}$$

$$\rho_v = \frac{\sqrt{\varepsilon_r - (k_{cv}/k_0)^2} - \varepsilon_r\sqrt{1-(k_{cv}/k_0)^2}}{\sqrt{\varepsilon_r - (k_{cv}/k_0)^2} + \varepsilon_r\sqrt{1-(k_{cv}/k_0)^2}}, \tag{2.48}$$

$$\rho_v = \frac{1-\sqrt{\varepsilon_r}}{1+\sqrt{\varepsilon_r}}. \tag{2.49}$$

With the help of above equations, one can obtain transmission, reflection and absorption coefficients for the disc type window as follows:

$$T = \frac{T_0(1-2R_0\cos(2\Phi)+R_0^2)}{1-2R_0T_0\cos(2\beta_{\varepsilon v}d_w-2\varphi)+R_0^2T_0^2}, \tag{2.50}$$

$$R = \frac{R_0(1-2T_0\cos(2\beta_{\varepsilon v}d_w)+T_0^2)}{1-2R_0T_0\cos(2\beta_{\varepsilon v}d_w-2\varphi)+R_0^2T_0^2} \tag{2.51}$$

$$A = \frac{1-R_0-T_0-R_0T_0^2-R_0^2T_0+R_0^2T_0^2-2R_0T_0(\cos(2\beta_{\varepsilon v}d_w-2\Phi)-\cos(2\beta_{\varepsilon v}d_w)-\cos(2\Phi))}{1-2R_0T_0\cos(2\beta_{\varepsilon v}d_w-2\varphi)+R_0^2T_0^2}. \tag{2.52}$$

Here, $R_0 = |\rho_V|^2, \Phi = \arg\rho_v, T_0 = e^{-2\alpha_{\varepsilon v}d_w}$. By using the above mentioned analysis, one can easily design an RF window operating at the single or multiple frequencies for any of the incoming modes, either TE/TM or TEM_{00} mode. In some cases, multi dielectric regions are used for improvement in the performance, for such cases, the net scattering matrix of the system is obtained by cascading the individual matrixes.

2.5.2. Results and Discussion

In the present work, considering various window materials, the RF window is designed. In all the designs, a single disc of dielectric material is considered as well the incident mode is chosen as Gaussian beam mode, i.e., TEM_{00}. Since, for the TEM_{00} mode, the radius of window does not affect the window characteristics, hence a window of radius 32 mm is selected. The material properties are tabulated in Table.2.5. The

reflection and transmission characteristics versus frequency for various disc thicknesses *d* are determined and plotted in Figures. 2.14 -2.16.

Table2.5: Material properties used for RF window design [Link *et al.* (1993)]

Material	Frequency	Permittivity	Loss tangent
Born nitride (BN)	95GHz	4.7	115×10^{-5}
Sapphire	95GHz	9.4	20×10^{-5}
CVD	95GHz	5.67	2×10^{-5}

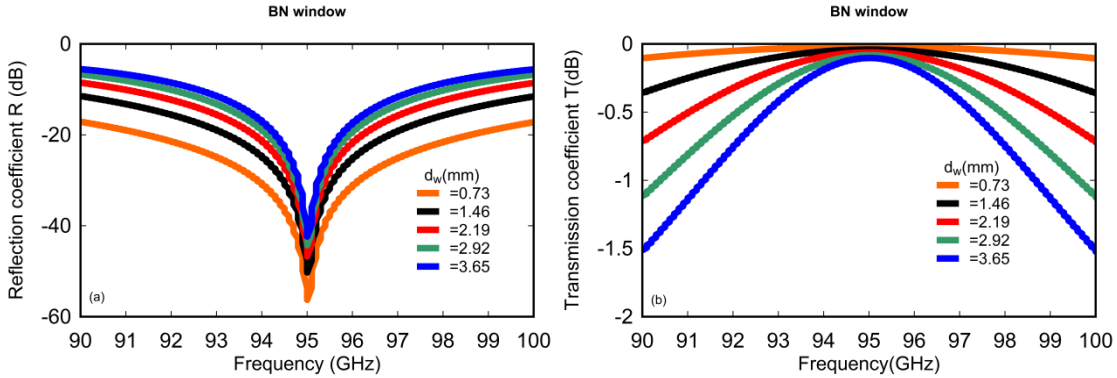

Figure2.14: (a) Reflection characteristics versus frequency (b) Transmission characteristics versus frequency for BN Window at various disc thicknesses d_w.

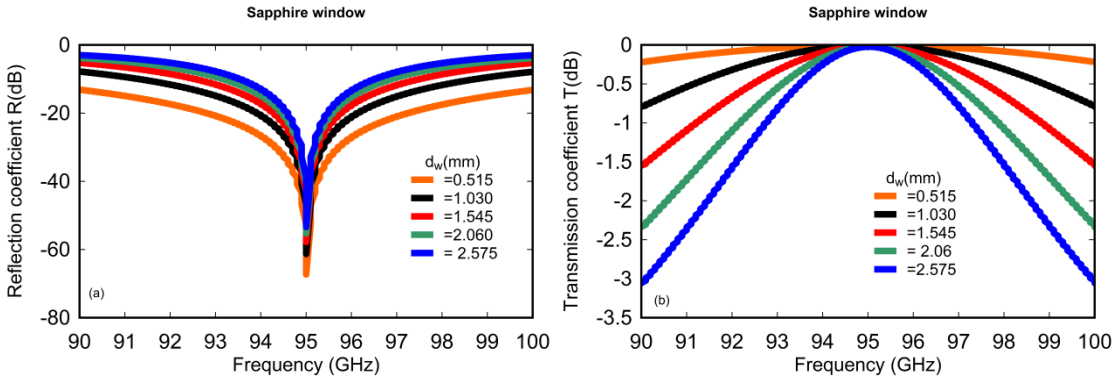

Figure2.15: (a) Reflection characteristics versus frequency (b) Transmission characteristics versus frequency for Sapphire Window at various disc thicknesses d_w.

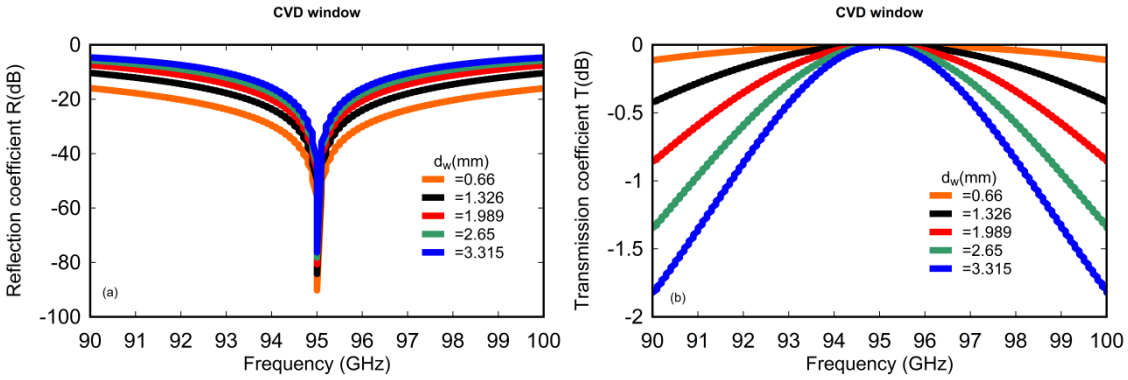

Figure 2.16: (a) Reflection characteristics versus frequency (b) Transmission characteristics versus frequency for CVD Window at various disc thicknesses d_w.

It can be observed that, in all the designs, as the thickness of the window d increases, the amount of reflection increases as well as the frequency range of maximum transmission coefficient also reduces that leads to the increment of the absorption coefficient. Though, all the designs show good reflection and transmission characteristics but depends on the range of power levels and optimum cost, the window material has to be selected. By studying the thermo mechanical behaviour of these windows, the final call can be taken based on the values of heat load (due to RF power absorption) and deflection, and higher tensile stress. Though this is kept out of the scope of the present study.

2.6. Conclusions

In the present chapter, Chapter 2, the advantages of an internal quasi-optical mode converter at high power high frequency gyrotrons are discussed. The basic theory used for the design, analysis of Vlasov mode launchers is described. Then, using the presented theory, the Vlasov type quasioptical mode launcher design parameters for the 95GHz $TE_{6,2}$ and 95GHz, $TE_{10,4}$ mode are calculated. Considering the presence of strong fields near the Vlasov cut, it has been shown that this leads to the severe

diffraction losses which in turn effects the conversion efficiency as well as the requirement of larger reflector geometries, limits the usage of Vlasov launcher to the whispering gallery modes. Then, design and analysis of modified Vlasov launcher, i.e., Denisov launcher has been also presented. The coupled mode theory used for the calculations of mode couplings due to irregularities as well the calculations of wall field intensities has been presented.

Using the analytical method proposed by Blank *et al.* (1994) the performance of the 110GHz, $TE_{22,6}$ mode gyrotron QOM launcher performance has been studied by considering four and eight satellite modes. It is found that consideration of more satellite modes gives better view of mode couplings due to dimples/irregularities in the launcher. Then, a computer code using MATLAB has been developed using the analytical approach developed here for the dimpled launcher. For the $TE_{10,4}$ 95GHz gyrotron, Denisov mode launcher design is performed manually using this code and by changing the launcher profile and confirming by observing the mode variation profile and Gaussian content at the launcher cut, since we do not have access to the popular LOT code generally used for this purpose. And the wall field's intensity profiles show a good Gaussian beam on the launcher cut has been observed.

Furthermore, the analysis and design of the disc type output windows used in gyrotrons are presented. Using the standard analytical approach and expressions, considering various window materials, the reflection and transmission versus frequency characteristics have been determined for the various cavity thicknesses. It has been found that as the thickness increases the amount of refection and the transmission coefficients are going against to the desired qualities of a window. Based on the amount of input power, the thickness of the material is needs to be chosen so that it can with

stand for the heat load generated by the RF power. However, thermo mechanical analysis of the windows has been kept out of the scope of the present work.